Journal of Geophysical Research: Oceans

RESEARCH ARTICLE
10.1029/2018JC014457

Key Points:
- Seawater is comprised dominantly (75–85%) of the hydrogen bonded pentamer $(H_2O)_5$
- The simple H_2O molecule exists in temperature-controlled equilibrium with the dominant $(H_2O)_5$ species
- Pressure forces the $(H_2O)_5$ species into a lower-volume nested state

Supporting Information:
- Supporting Information S1
- Table S1

Correspondence to:
P. G. Brewer,
brpe@mbari.org

Citation:
Brewer, P. G., Peltzer, E. T., & Walz, P. M. (2018). How much H_2O is there in the ocean? The structure of water in sea water. *Journal of Geophysical Research: Oceans*, *123*. https://doi.org/10.1029/2018JC014457

Received 8 AUG 2018
Accepted 20 NOV 2018
Accepted article online 30 NOV 2018

How Much H_2O Is There in the Ocean? The Structure of Water in Sea Water

Peter G. Brewer[1], Edward T. Peltzer[1], and Peter M. Walz[1]

[1]MBARI, Moss Landing, CA, USA

Abstract We report on laboratory and field Raman spectroscopy experiments on the structure of water in sea water and describe this as a function of temperature and pressure. The Raman spectrum of water/seawater is dominated by the water stretching mode band with a frequency shift in the range 2,800–3,800 cm^{-1}. Here the hydrogen bonded (HB) clusters of several water molecules and nonhydrogen bonded (nHB, singlet H_2O) forms are revealed with an isoskedastic point, similar to the isosbestic point for pH sensitive dyes. This band can be deconvolved into five Gaussian peaks, each with a specific spectroscopic assignment. We find that within the temperature range of 0–40 °C the vastly greater mass and volume of ocean water (78–85%) is in the HB forms, dominantly as $(H_2O)_5$. Without hydrogen bonding there would be no ocean, and nowhere in the bulk ocean does the simple H_2O molecule exceed 20% of the total. The fraction of water molecules in the solvation shell around ions in seawater represents a third type of water, bound to an ion but not hydrogen bonded. Approximately 6% of the water molecules present at 35 salinity are in this form, and their concentration is not affected by temperature or pressure. The HB forms are a continuum of species in rapid exchange. The fraction of nHB is driven solely by temperature. We find no evidence that increased pressure changes the population of the free singlet nHB molecule; pressure drives the dominantly $(H_2O)_5$ population toward a lower volume, nested, molecular state.

Plain Language Summary For over 50 years ocean scientists have represented the important physical properties of sea water as a collection of bulk fluid coefficients that simply provided a statistical fit to the observed compressibility, sound speed, etc.—but with no underlying molecular basis. Sea water is 96.5% water, and for over 50 years chemists describing the molecular physics of pure water have evolved an understanding that water is composed of a temperature-driven balance between the hydrogen bonded and nonhydrogen bonded forms, but this knowledge has not been applied to the oceans—the largest body of water on Earth. Here we link these two fields by using laser Raman spectroscopy. We show that by far the greater volume of the ocean—some 78–85% is composed of the hydrogen bonded form $(H_2O)_5$. Without this water would not be liquid and we would literally have no ocean at all. With this knowledge we are better able to understand the processes occurring under climate-driven ocean warming.

1. Introduction

How much H_2O is there in the ocean? The question is surprisingly hard to answer because a large fraction of the water molecules are hydrogen bonded together forming molecular clusters. Rather little of the liquid water exists as the singlet H_2O molecule. Water exists dominantly as a bimolecular fluid in which the hydrogen bonded clusters and nonhydrogen bonded forms are in a temperature-controlled dynamic equilibrium. Sea water is dominantly (~96.5%) water, and over the last 50 years there has arisen a large, lively, and powerful literature on the chemical physics of water (a simple online search for "scholarly articles on the structure of water" reveals some 19M hits) yet very little of this has crossed over to the ocean sciences.

Here we briefly review this body of knowledge, and we report on both laboratory and field spectroscopic experiments to test how well the knowledge of hydrogen bonding in pure water can be translated into the medium of sea water. We describe the chemical structures that underlie the physical properties of sea water and assess their abundance in the ocean water column.

In simplest terms, the structure of water is the result of the balance between the thermal forces pulling water clusters apart and the chemical forces holding these clusters together. The dominant chemical force holding water molecules together is the hydrogen bond, and within the oceanographic range water is in a state of

temperature-controlled equilibrium between the hydrogen bonded (HB) and the nonhydrogen bonded (nHB) forms. The nHB form is simply the free H_2O molecule, and the various (HB) forms exist in a rapidly exchanging continuum of configurations of which the dominant form is the tetrahedral pentamer $(H_2O)_5$ (Brewer et al., 2017; Carey & Korenowski, 1998; Smith et al., 2005; Walrafen, 1964; Walrafen et al., 1986). It is the presence of this tetrahedral form, known as the Walrafen pentamer, that causes water to be liquid and it exerts the principal control on the physical properties of water and sea water. Without HB forms there would literally be no ocean.

This well-established phenomenon of dominant end members represented by the H_2O and $(H_2O)_5$ forms connected by a continuum of rapidly exchanging intermediate forms (dimers, trimers, and tetramers) is essential for understanding the properties of water and sea water. It is this that allows the molecular population of the fluid to adjust instantaneously to even very small changes in *T* and *P*—so that a passing cloud, or a rise of tide, are instantly accommodated without latency or threshold value.

An essential tool for probing these structures is Raman spectroscopy, and with the advent of robust and sophisticated Raman spectrometers for deep sea deployment (Brewer et al., 2004; Zhang et al., 2012) it has now become possible to begin to merge laboratory and field data on the structures of water in seawater with basic theory.

The ionic speciation of seawater salts has long been recognized as critical to understanding seawater chemistry, but the speciation of water itself has essentially been ignored and it has been treated simply as a bulk fluid. This tactic has allowed progress by providing a fit to experimental data, but it conveys little knowledge of the underlying molecular basis. For example, recent work shows that with even a little insight into chemical physics a significant advance in simplicity and accuracy in representing sound speed in sea water is possible (Brewer et al., 2015) simply by treating the compressional wave as a pressure perturbation of the water equilibrium state as represented by a van 't Hoff function. Here we apply similar principles.

We have previously shown that the basic water molecular partition between HB and nHB forms can be observed directly in the field and that the strength of the hydrogen bond of water in sea water can be determined (Brewer et al., 2017). In these early field observations the effects of temperature (*T*) and salinity (*S*) were comingled. We also had an indication that below the thermocline the observed spectra of the ratio of HB to nHB forms appeared to be nearly constant with depth suggesting that pressure (*P*) had little effect on this ratio.

We now extend these observations and provide both laboratory and field data on the *T* and *P* dependence of the equilibrium between HB and nHB forms in the ocean water column, and directly evaluate their abundance by estimation of the Raman cross sections of these species. The work has relevance to many properties of oceanic interest: it is the nHB form in surface waters that exchanges with the atmosphere, and it is the HB structure of water that controls the surface tension and the speed of sound. Water structure controls viscosity (Stanley & Batten, 1969) with importance for the energetics of life at low Reynolds number (Purcell, 1976).

2. Background

2.1. Early Ocean Measurements

The earliest reported field use of the Raman spectrum of ocean water is by Leonard et al. (1977). Here a time-gated pulsed laser system was installed on the RV *Makai* and measurements made by projecting the beam vertically down through air into the waters of the Annisquam River, Massachusetts, estuary. Comparisons of temperature estimated between laboratory and field data were made by assuming that "liquid water exists in at least two forms: monomers and dimers" and that these are in equilibrium as a function of temperature. From these first findings they proposed development of an aircraft-based Raman water temperature measurement system. That promise was fulfilled and Leonard et al. (1979) reported aircraft-based measurements with a 532-nm laser pulsed at 10 ns time gating and assuming the same two-component structure achieved ±2 °C precision.

This effort was extended in a series of laboratory measurements on water and on synthetic sea water by Becucci et al. (1999) who confirmed the accuracy of the measurement, again using a simple two-component fit. The deconvolution of the large water stretching mode band into two Gaussians was ad hoc, and no specific spectroscopic assignments were made. Importantly, Becucci et al. (1999) noted the influence of salinity

on the observed ratio of the two Gaussians but were not able to separate the temperature and salinity effects. That is only by knowing salinity could one then predict temperature from the observed ratios; the temperature and salinity effect on the observed Raman ratio resulted in exactly parallel lines. The effect of the added salts on the observed Gaussian ratios over the range 0–38 salinity was quite large with an apparent value of ~12%; but since the Raman cross sections of the species are not known this is only a relative value.

No specific chemical mechanism for the observed correlation with salinity was reported. Since this technique does not directly observe the salt ions, it seems likely that the salinity effect is due to the presence of a third form of water structure: those water molecules not in free solution, but bound in the solvation shell around sea salt ions. Raman X-ray experiments on simple salt solutions (Waluyo et al., 2011, 2014) show that the strength of the bonding has only a very weak dependence on temperature and that the number of water molecules in the solvation shell has no temperature dependence; the quantity of "solvation water" is simply a linear function of the molar concentration of salts present.

2.2. The Chemical Physics of Pure Water

Walrafen (1964) provided early Raman spectroscopic evidence of water structure and described the results in terms of a dominant five-molecule hydrogen bonded tetrahedral structure. He described the variations in intensity of intermolecular vibrations with temperature, noted that two hydrogen bonds are broken when one H_2O molecule is liberated from a tetrahedral structure, and also that "the degree of association of water at 0°C obtained in this work ...89.5%, is in close agreement …" with other work. Thus, pure water at the freezing point is 90% in the HB form and this provides a useful system point for quantification. Walrafen (1964) also carried out an early investigation of the effect of added salt species on band intensity noting that "the fact that intensity decreases were observed for all electrolytes studied indicates that O-H···H units were broken"; that is, that the effect is dominantly on the population of the HB forms. This is not surprising since the HB forms are by far the most abundant species.

Walrafen (1967) and Walrafen et al. (1986) later showed the existence of apparent isosbestic points (technically isoskedastic points since the Raman effect is the molecular scattering of light as opposed to the absorption of light) in the Raman spectrum of liquid water, confirming what is essentially a two-component state with the temperature-dependent equilibrium of HB and nHB forms. This has been contested over the years, but recent work strongly supports this conclusion (Canpolat et al., 1998; Carey & Korenowski, 1998) in which the basic equilibrium is between $[H_2O] \leftrightarrow [H_2O]_n$ where n is typically 5 representing the tetrahedral pentamer. Strong evidence exists for the $(H_2O)_5$ species to exist in continuum with the presence of a population of rapidly exchanging other (dimer, trimer, tetramer, etc.) transient forms (Keutsch & Saykally, 2001) with the tetrahedral form dominant (Smith et al., 2005). One usefully succinct description of the water state is that given by Kumar et al. (2007) who report that their results are "consistent with the traditional idea that water is highly disordered, but with more or less tetrahedral local symmetry, with at least 3 H bonds per molecule, some of which are stronger than others, and a majority of water molecules are double donors."

The Raman spectrum of liquid water is dominated by the stretching mode band complex in the region 2,800–3,800 cm^{-1}. This complex can be deconvolved into five Gaussians (Furić et al., 2000; Walrafen et al., 1986) each with a specific spectral assignment. Walrafen (1964) was the first to attempt this and he identified three bands between 2,800 and 3,800 cm^{-1}. In subsequent papers he reported four bands (Walrafen, 1967) and five bands (Walrafen et al., 1986). More recently Carey and Korenowski (1998) and Furić et al., (2000) have identified five Gaussian peaks (Table 1). One of these bands, which is centered at 3,052 cm^{-1}, is attributable to the $2\nu_2$ overtone of the bending vibration of the singlet water molecule (Furić et al., 2000) and need not be considered further here. The remaining four bands reflect the population of the HB and nHB forms of water.

The Raman frequency shifts of these bands change very little with temperature or pressure within the normal oceanographic range, but the band areas do (Walrafen, 1967). For pure water the band centered at 3,220 cm^{-1} shows a decrease in area with rising temperature indicating association with an HB form; the bands centered at 3,390 cm^{-1} and 3,485 cm^{-1} both increase in area with rising T showing their association with the nHB form. The remaining band centered at 3,624 cm^{-1} shows a small decrease in area with rising T and was not included in the calculation of the equilibrium ratio (K) in our earlier study (Brewer et al., 2017), although here we have made use of it.

Table 1
Nominal Raman Shifts (cm^{-1}) for Water Stretching Bands From Multiple Sources

Source	Sample	Peak 1	Peak 2	Peak 3	Peak 4	Peak 5
Walrafen (1964)	Pure water		3,225	3,450		3,630
Walrafen (1967)	Pure water		3,225–3,260	3,425–3,450	3,520–3,550	3,612–3,625
Walrafen et al. (1986)	Pure water	3,110	3,212	3,383	3,520	3,620
Carey and Korenowski (1998)	Pure water ([a])	3,051	3,233	3,393	3,511	3,628
Furić et al. (2000)	Synthetic sea water	3,217	3,274	3,452	3,568	3,648
Brewer et al. (2017)	Real sea water	3,049.9	3,220.2	3,390.0	3,485.1	3,624.2
This work:	Pure water	3,052.0	3,220.0	3,394.0	3,502.0	3,624.0
	Sea water	3,051.7	3,222.3	3,388.6	3,486.5	3,623.9
	Diff (sw − pw)	−0.3	2.3	−5.4	−15.5	−0.1

Note. All samples were run at normal lab temperatures and 1 atm total pressure except as noted.
[a]At 22 °C and 256 bar.

The ratio of these forms can be described as a van 't Hoff function (Carey & Korenowski, 1998; Smith et al., 2005) which defines the equilibrium constant K for the balance of the HB versus nHB forms. A plot of the natural log of the ratio of the sum of the two nHB band areas divided by the sum of the two HB band areas versus the inverse of absolute temperature yields a measure of the strength of the hydrogen bond. The hydrogen bond enthalpy has been calculated in this way both for pure water (2.53 kcal/mol; Carey & Korenowski, 1998) and for sea water (2.48 kcal/mol; Brewer et al., 2017).

We note that the bond enthalpy calculated in this way is essentially based on a simple two-component model, yet there is also a population of other water cluster species (dimer, trimer, tetramer, etc.) that are not accommodated in this simplified form. These have polarities intermediate between the end member species and thus affect the Raman observations. Smith et al. (2005) observe and accommodate for those species and report a value of 2.0 kcal/mol for pure water. Silverstein et al. (2000) have carefully reviewed many of the prior estimates of H-bond enthalpy and reported a range from 1.5 to 2.9 kcal/mol, with their preferred value being 1.9 kcal/mol.

The HB tetrahedral pentameter is the only fully three-dimensional structure and it is highly favored as a local energy minimum state (Walrafen, 1964). It is represented by the ~3 times greater length of the hydrogen bond (280 pm) versus the covalent O-H bond (96 pm), and the far weaker bond strength; based upon a very simple spherical approximation the HB pentamer has approximately some 60 times the volume of a single nHB molecule, and is 10 times larger than the five individual molecules that comprise the pentamer. Nonetheless, the pentamer form is the lowest volume possible arrangement, and it is the primary reason that water exists in the liquid state. Both the free nHB molecule and the tetrahedral pentameter are highly incompressible. Keutsch and Saykally (2001) describe the dimer, trimer, and tetramer forms also as very nearly planar and rigid.

The effect of pressure is to drive the system to a lower volume state, but the efforts to describe this, as reported in the chemical physics literature, typically cover a far wider range of *T* and *P* than what occurs in the ocean and are heavily focused on the high-pressure properties of ices and associated structural heterogeneities in the liquid (Khoshtariya et al., 2004; Mishima & Stanley, 1998).

The most practical description of pressure effects is that of Canpolat et al. (1998), who carried out molecular dynamics calculations of a simple nearest neighbor model and found evidence for the nesting of adjacent pentamers to form two-pentamer clusters. They report that "when pressure increases we expect the number of non-hydrogen bonded pentamers to increase" (their Figure 1d)—that is, the population of solo $(H_2O)_5$ species is diminished and replaced by an increase in the lower volume, nested, $[(H_2O)_5]_2$ cluster.

The overall picture is therefore that, of all the molecular species present, it is the $(H_2O)_5$ pentamer that is most susceptible to pressure via simple nesting with no formation, or breaking, of hydrogen bonds; this is, in brief, the reason why warm waters, with less of the $(H_2O)_5$ form, are less compressible than cold waters. The pentamer oxygens interact in the model (Canpolat et al., 1998) by finding a Lennard-Jones potential minimum calculated using water values taken from Walrafen et al. (1986).

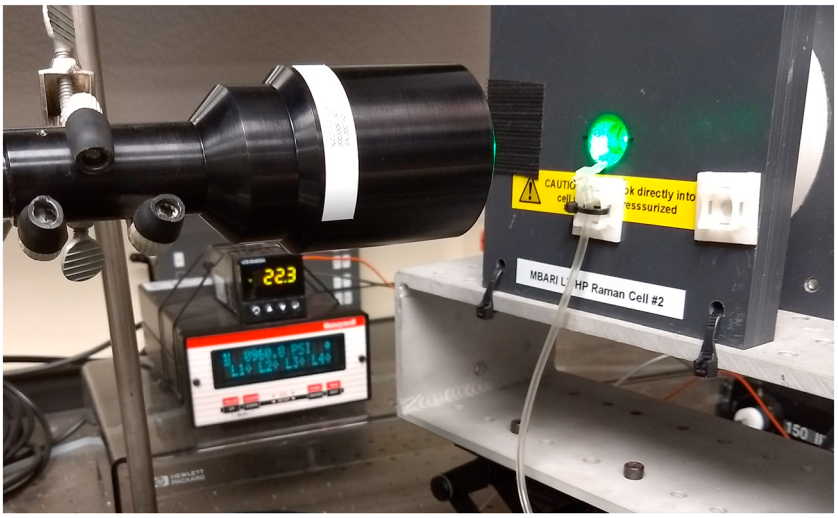

Figure 1. The 532-nm Raman laser focused on the sapphire window of the pressure cell. The clear tube at the bottom of the pressure cell provides a stream of dry air to keep condensation off the window at lower temperatures.

3. Experimental

We have performed a series of both laboratory and field Raman measurements to examine the changing proportions of the HB and nHB forms of pure water, and water in sea water, to investigate the properties described above.

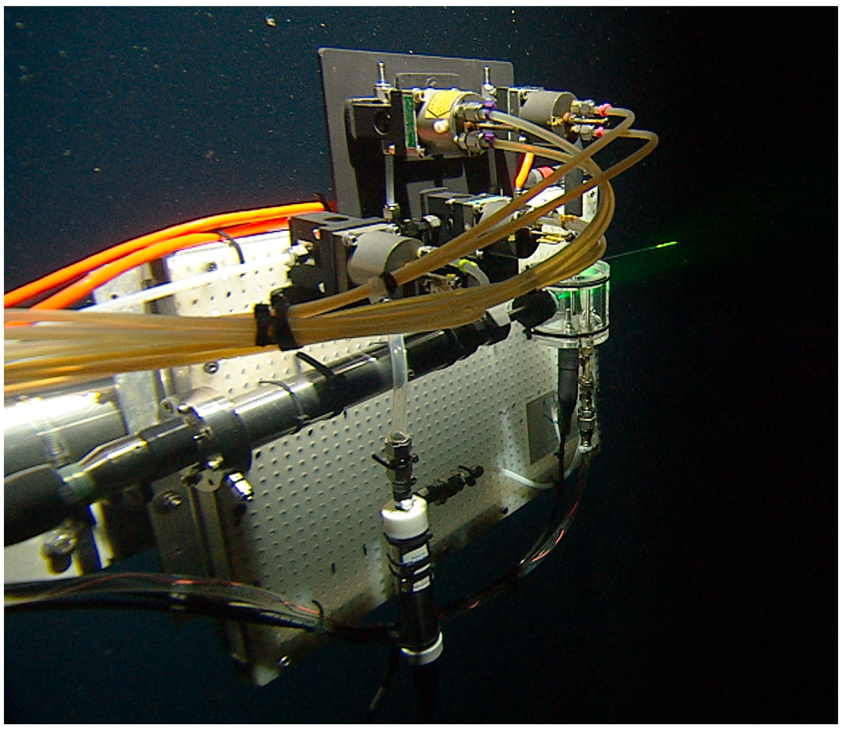

Figure 2. A field experiment in progress. The laser is mounted horizontally and the green laser beam can be seen inside the control cell in the package deployed on the vehicle swing arm. The cell contains natural sea water (S_A = 34.671). Mounted vertically through the bottom of the cell is a heater powered by the vehicle, and inside the cell is a thermistor for recording temperature. Experimental data are transmitted through the tether and recorded in the ship's control room.

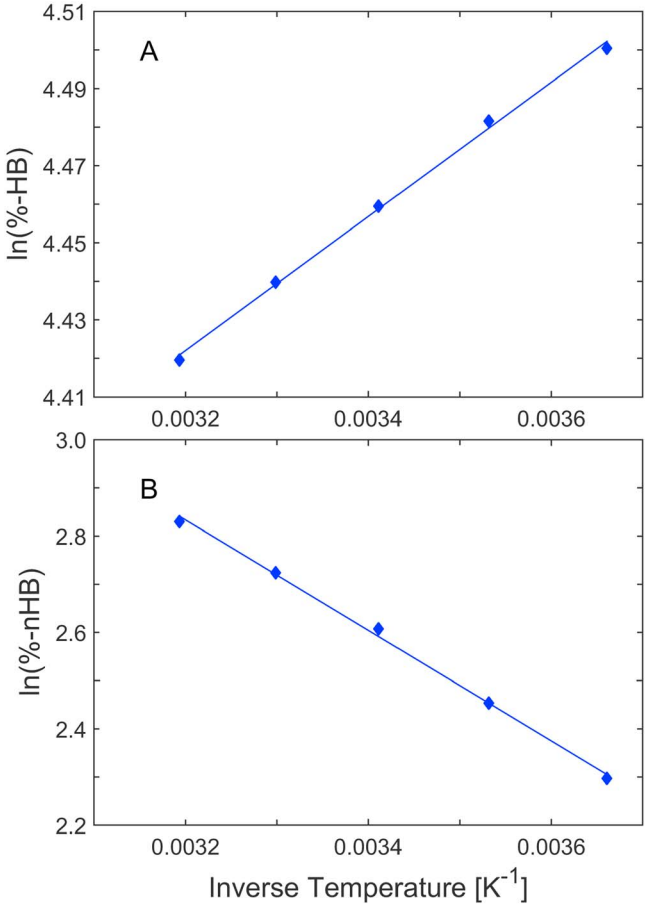

Figure 3. van 't Hoff plots of the calculated molar concentrations of both the hydrogen bonded form (a) and the singlet H_2O form (b) for pure water at 1 atm based upon the sum of the respective peak areas and the relative molar response factor.

The DORISS 2 system we use has been described in detail earlier (Zhang et al., 2012); it is built on a laboratory laser Raman spectrometer from Kaiser Optical Systems, Inc (KOSI). The core components are a KOSI Raman RXN optical bench f/1.8i spectrometer, a front-illuminated Peltier cooled 2048×512 charge-coupled device camera by Andor Technology (Belfast, UK), and a Coherent Compass 315-M 532-nm frequency-doubled Nd:YAG laser. The spectrum is split into two lines on the face of the camera by a duplex grating, enabling measurement of the full spectral range from 200 to 4,400 cm^{-1} with ~4 cm^{-1} optical resolution and an approximate 1 cm^{-1}/pixel mapping. Neon and tungsten lamps are used for wavelength and intensity calibration prior to field deployment. Real time camera control options and spectral data acquisition are handled using the KOSI "Holograms" software package.

3.1. Laboratory Measurements

We have carried out careful laboratory measurements (Figure 1) of the Raman spectrum of pure water and sea water (S_A = 34.524) over a range of five temperatures from 0 to 40 °C, and for seven pressures from 0 to 1,500 psig in 250 psig steps, by well-established pressure cell techniques (Brewer et al., 2017). Pressure was controlled to ±1 psig by adjustment of a screw-thread piston ram attached to a Parker pneumatic piston. Temperature was controlled to ±0.1 °C with a constant temperature bath recirculating water and coolant to a water jacket surrounding the 1-cm^3 volume pressure cell fitted with a sapphire window (Sam D. Colgate Inc., Gainesville, FL).

We have also carried out measurements on the effect of salinity at constant temperature over the range S_A = 0–34.524 by a five-step simple dilution of the same sea water sample with pure water.

3.2. Field Measurements

Previously we have carried out a series of field experiments in offshore California waters using the remotely operated vehicles (ROVs) *Ventana* and *Doc Ricketts* as the experimental platforms for Raman spectrometer deployment. Direct measurements of open water spectra were acquired simply by exposing the Raman probe head to sea water and recording observations at various depths during the ROV dives. Here we gained knowledge of the natural ocean water column state, but with the effects of changing *T*, *P*, and *S* comingled (Brewer et al., 2017).

We have also carried out a field version of the laboratory pressure cell measurements by constructing a controllably heated cell in which the laser probe head was installed (Figure 2). This cell was filled with either

Table 2
The Quantities of Hydrogen Bonded (HB) and nHB Forms in Pure Water Based on a Simple van 't Hoff Relationship and the Raman Cross Sections Estimated Here

S pss-78	*T* °C	*P* (gage) dbar	% HB	Conc (moles/L)		Conc (moles/kg)	
				[HB]	[nHB]	[HB]	[nHB]
0.000	0.00	0.0000	90.0	49.95	5.55	49.96	5.55
0.000	10.00	0.0000	88.4	49.03	6.46	49.04	6.46
0.000	20.00	0.0000	86.6	47.99	7.42	48.08	7.43
0.000	30.00	0.0000	84.8	46.86	8.40	47.07	8.44
0.000	40.00	0.0000	82.9	45.67	9.41	46.03	9.48

Note. Experimentally determined quantities as both molar and molal concentrations, and percentages, of the H-bonded and single H_2O forms in pure water as a function of temperature at 1 atm. In pure water the only form of bonding is through hydrogen bonds. The calculations are based on the estimate of Walrafen (1964) of 90% HB form at 0 °C.

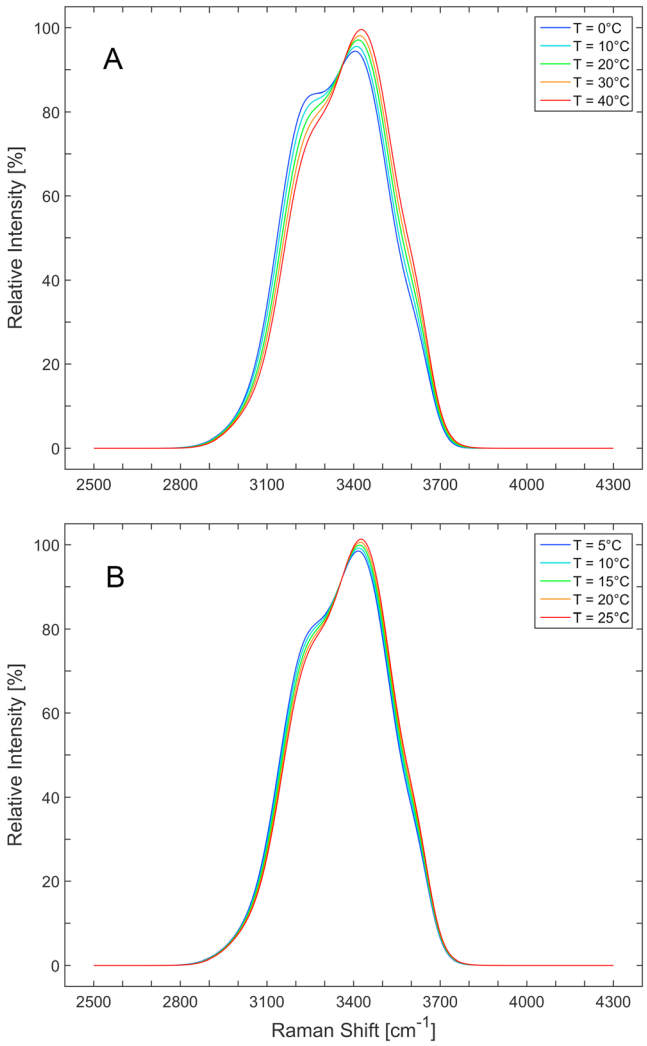

Figure 4. Expanded view of a series of Raman spectra of pure water (a) obtained in the laboratory at 1 atm and of natural sea water (b) obtained at 1,000-m depth (P = 1,012 dbar) within a temperature-controlled cell as shown in Figure 2. The sea water was at a constant salinity (S_P = 34.490, S_A = 34.671); note that the temperature range achievable in the field experiment was less than that on the pure water sample in the laboratory. Both data sets show an isoskedastic point: at 3,362 ± 3 cm^{-1} for pure water and 3,356 ± 3 cm^{-1} for sea water. See text for an explanation of the change in Raman shift for the isoskedastic point.

pure water, or natural sea water, and transported by the ROV to several depths in the water column, where an experimental increase in temperature at the local pressure and at constant salinity was created and the Raman spectra observed. The advantage of this approach is the elimination of possible distortions, focusing variations, and polarizations that can occur in focusing the laser beam in air through the laboratory cell sapphire window; such effects are well known as experimental challenges in the laboratory (Smith et al., 2005; Walrafen et al., 1986).

3.3. Spectral Processing

Refinement in signal processing to extract accurate information from the spectra is critical. The most commonly used program for processing Raman spectra is the GRAMS software package and forms of this have been used by us for many of the geochemical systems (methane hydrates, dissolved CH_4, SO_4^{2-}, etc.) that we have examined (Zhang et al., 2012).

In our experience the GRAMS software package presents some challenges where there are multiple overlapping peaks within a spectral band that require deconvolution, as in the water stretching mode band which consists of five overlapping peaks in the region 2,800–3,800 cm^{-1}, or where complex baseline trends from fluorescent species in natural waters are found. For this reason we have developed innovative MATLAB® routines for greater precision in signal processing. Here we use several of these techniques for Raman spectrum analysis. In earlier work (Brewer et al., 2017) we have provided a description of the deconvolving of the water stretching mode band into its five-component Gaussians, with spectroscopic assignments, Raman shifts, and peak relative areas, and therefore we do not repeat these details here.

4. Results

4.1. Converting the Observed Raman Peak Areas to Concentrations

The procedures above yield the observed band areas for the HB and nHB forms of water over a wide span of T and P. Since we do not yet know the Raman cross sections for these bands we can so far establish only relative values, but for ocean science true concentrations are required. The intensity of Raman scattering is closely tied to bond polarizability, and since the single H_2O molecule is strongly polarized we may expect large differences in sensitivity of detection. We therefore need some fixed point from which to establish the true proportions of the species, and once this is found, true concentrations can be detected since the relationship between peak area and concentration is linear (e.g,. Zhang et al., 2011).

We have recently solved a very similar problem (Peltzer et al., 2016) for the pH-dependent equilibrium of the H_2S-HS^- pair. Here the known point was established by the fact that these species are equal in concentration at the point where pH = pK, and spectra bracketing this point can be readily determined. In that experiment we found that the Raman cross section for the more polarized HS^- species was 1.56 times greater than that of the H_2S species.

One way to approach this for quantification of the water system is derived from observations of the melting of ice. Pauling (1960) noted that "the small value of 1.44 kcal/mol of the enthalpy of fusion of ice shows that on melting only about 15% of the hydrogen bonds are broken." Walrafen (1964) refined this estimate and reported that at the freezing point of pure water 90% of the fluid is in the HB form. At the freezing point the water structures are dominantly a mixture of pentamers and hexamers, and the resulting increase in volume accounts for the well-known decrease in water density below 4 °C. This result is at 1-atm pressure; it is unlikely that the Raman cross sections are a function of P, since this does not change bond polarizability.

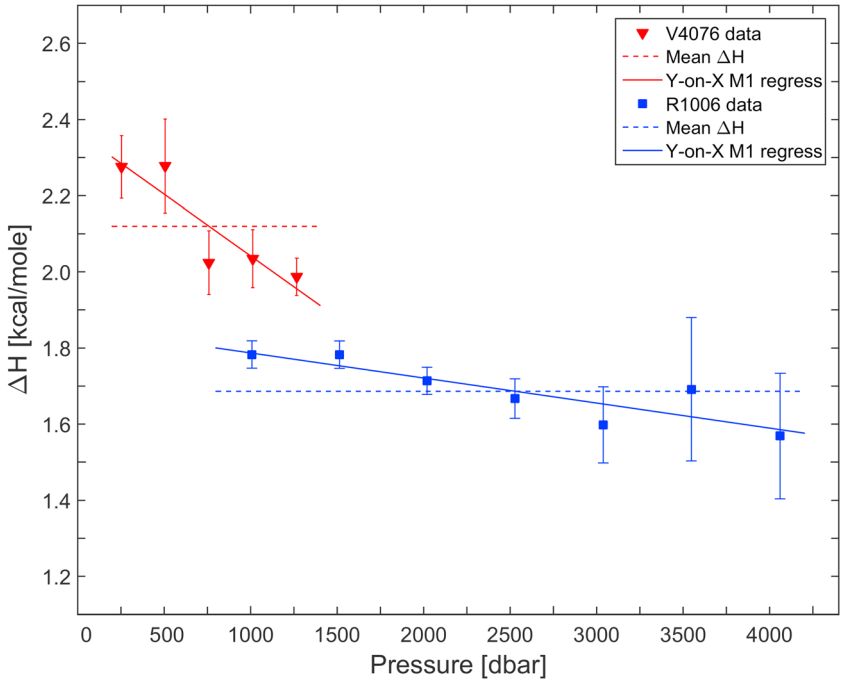

Figure 5. Estimated change in sea water ΔH as a function of pressure from a series of heated cell experiments carried out at several depths at sea as shown in Figure 2. These results are within our limits of detection, but the physical basis for this remains unclear.

By setting the observed band areas at 0 °C for the nHB forms in pure water as representing 10% of the water present, and by setting the observed band areas for the HB forms as representing 90% of the water present and using the algebraic formulation described in detail in the supporting information, we calculate a relative response factor of 10.8 times for the detection of the nHB versus the HB forms. This is strong testimony both to the high polarity of the nHB H_2O molecule, and the remarkable minimization of polarity afforded by the highly favored pentamer structure. The Raman bands, while dominated by the pentamer presence, also contain information from the slightly more polarized tetramer, trimer, and dimer forms inevitably present. Even though the nHB molecule is present at only 10–15% of the population, it is nonetheless revealed with high sensitivity.

In Figure 3 we show the van 't Hoff plots corresponding to these data. In Table 2 we report estimates of the molar concentration of water species in pure water as a function of temperature based upon the linear regressions in Figure 3 (for the regression coefficients, see the supporting information).

4.2. Field Results From the Heated Cell Experiments

In Figure 4 we show a series of spectra obtained from pure water in the lab cell at 1 atm and 0–40 °C, and sea water (S_P = 34.490, S_A = 34.671) in the heated cell at 1,000-m depth (P = 1,012.0 dbar) covering a range of 5–25 °C. The isoskedastic point that broadly defines the overlap of the population of HB and nHB forms is clearly seen at a Raman shift of 3,363 ± 3 cm^{-1} for pure water and 3,356 ± 3 cm^{-1} for sea water. This small shift in the temperature isoskedastic point is likely due to the presence of a third form of water in the sea water spectra: water molecules bound in the solvation shell around the salt ions in sea water (see below).

We have carefully examined the data obtained from the full series of heated cell experiments carried out in the field over a range of pressure. These experiments cover a range from 200 to 4,000 dbar and combine field work executed from both the ROV *Ventana* and ROV *Doc Ricketts*. We note that expedition staging required that these two field experiments were carried out with slightly different optical paths. From these combined data we calculate the apparent bond enthalpy (ΔH) in a manner identical to that reported in Brewer et al. (2017). We find a small but detectable trend toward lower ΔH with increasing pressure (Figure 5).

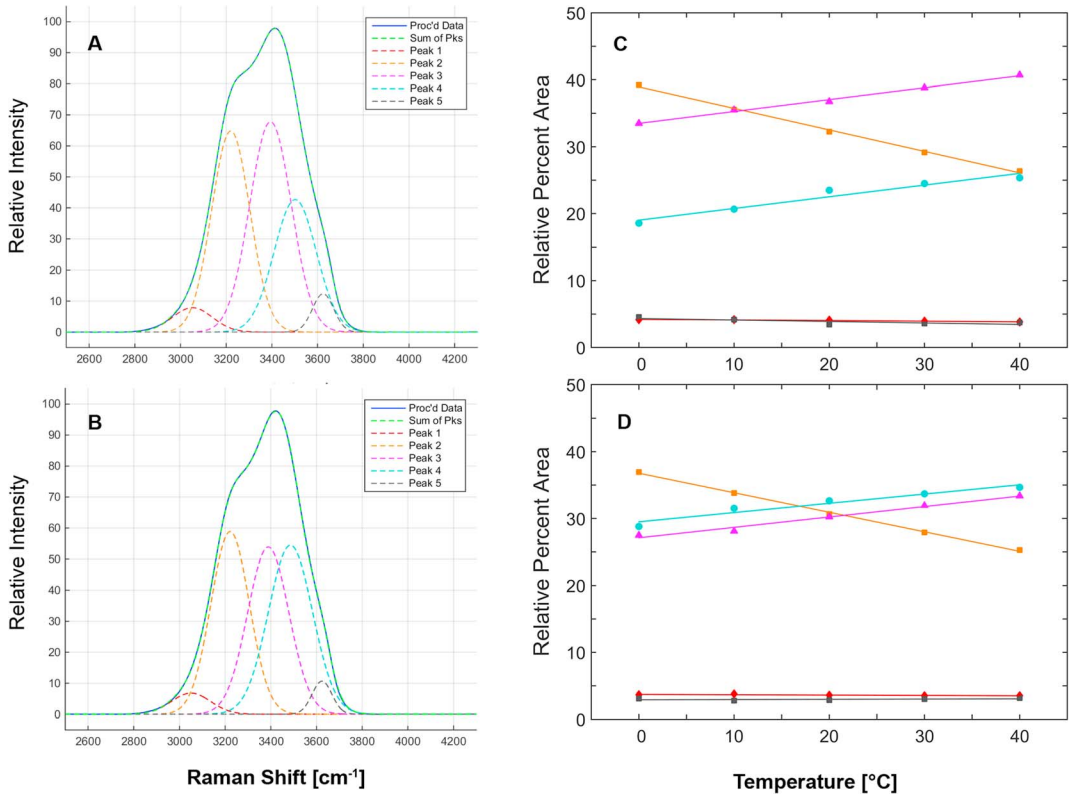

Figure 6. Comparisons of the spectra of pure water (a) and sea water (b) both at 20 °C. The spectra are deconvolved into their five Gaussian components. In the sea water sample peaks 3 and 4 associated with the single water molecule modes are reversed in peak area and height compared to the pure water spectra. In the right-hand panels (c and d) we show the temperature dependence of the areas of these same peaks by the red and blue lines that have a positive trend with *T*. In pure water peak 3 (red line; asymmetrical stretching) is dominant; in sea water peak 4 (blue line; symmetrical stretching) is dominant. The results clearly show the effect of ions in capturing water from the bulk fluid to populate the solvation shell.

It is unclear at this time what the basis for this observed trend is. The apparent ΔH values calculated appear low by comparison with laboratory results, and we recognize that there are differences in the optical path. Nonetheless, the observed trend is significant within the limits of the experiment and for the moment this remains as a curiosity. Recall that these are apparent values and that the simple two end member fit includes a range of intermediate species.

The details of isoskedastic points were carefully investigated by Robinson et al. (1999), who noted that pressure-induced isosbestic points could occur; but their data cover a pressure range far exceeding the normal oceanographic range and we find no evidence of that here.

5. Discussion

The spectra shown in Figure 6 contain multiple Gaussian components corresponding to the stretching modes of the various water structures. Bands 2 and 5 are from the HB forms and these decrease in area with increasing temperature; bands 3 and 4 are from the nHB forms and these increase in area with increasing temperature. This temperature effect is clearly seen in Figures 4, 6c, and 6d.

We find that the Raman frequency shifts of the individual components we observe by deconvolving the spectra for both pure water and sea water are not affected by temperature or pressure within the limits of our measurements. Comparing our observed shifts for pure water to those reported by others (Table 1) we find only minor differences, adding confidence to our peak assignments. This is critical for accurate comparison of spectral information obtained over wide *T* and *P* ranges in the field. In brief, the peaks we find do not move around—only their area changes as a result of the environmental conditions. The only small difference in wave number shift we observe in sea water compared to pure water is that for peaks 3 and 4. These

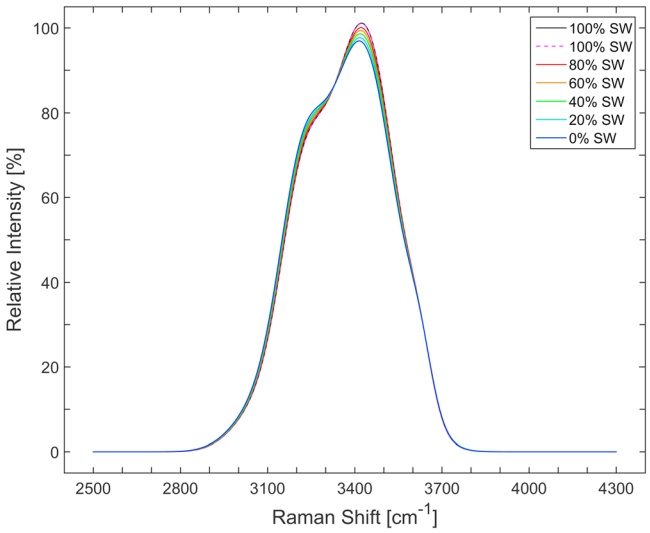

Figure 7. Laboratory data on the Raman spectra of sea water at various salinities showing the isoskedastic point at 3,329 cm^{-1} resulting from the saline perturbation of the fluid. Sea water (S_A = 34.524) was progressively diluted to obtain the spectra. Care was taken to correct for the changes in the small background natural fluorescence signal, and to normalize Raman intensity to a constant peak area. The effect arises since the ion solvation shells contain a third form of singlet water molecules, neither free nor hydrogen bonded but bound to the cations in a metal and ligand complex. These appear in the spectrum as an increase in nHB forms, with a concomitant decrease in the HB pool.

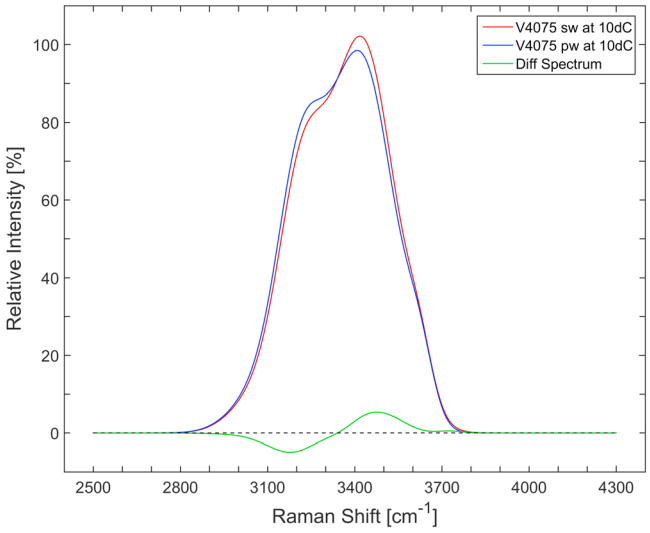

Figure 8. Spectra of pure water (blue line) and sea water (red line), and the difference spectrum (green line), at 10 °C obtained in the field under identical conditions. The result simply demonstrates the reduction in the total quantity of HB forms, and the increase in the combined free H_2O and H_2O molecules bound in the solvation shell. Recall that the Raman cross section on the nHB forms is 10.8 times that of the HB forms, but that the cross section of the molecules bound in the solvation shell is not known. It is very likely less than that of the free nHB form due to the small reduction in polarity. HB = hydrogen bonded; nHB – nonhydrogen bonded.

represent the non-HB forms, and the small change in Raman shift is likely due to the presence of nHB water in the hydration sheath around major ions where the polarity of the water molecule is affected compared to that in free solution.

While the Raman peaks do not shift in frequency with changing temperature and salinity, the peak areas do (see supporting information, Table S3). By examining the peak areas in more detail we can clearly observe the effects of temperature and salinity on the water structures (Figure 6).

The effects of temperature on the ratio of the HB and nHB forms have long been studied and are simply confirmed and quantified here. However, the information contained on the effects of salinity on the water structure is new. In Figures 6a and 6c we see the components of pure water. In Figures 6b and 6d for sea water we observe significant changes: peaks 3 and 4 are reversed in height compared to the pure water signal. This effect is maintained over the full range of temperatures observed.

The presence of sea salts provides the primary driver for the difference between the now well-known pure water spectra and the oceanic signal (Figures 6a and 6b. As with temperature, plots of the Raman spectra of sea water at various salinities at constant temperature show an isoskedastic point originating from the progressive increase of sea salts (Figure 7), although the interpretation of this must be very different from that of changes in temperature.

There is no single or specific Raman spectroscopic signature of the effects of any one saline component within the water band stretching region, but the overall effect is very clear. Anions such as SO_4^{2-}, NO_3^{-}, and CO_3^{2-} have direct Raman signals, but these lie far outside the spectral range we are considering here.

In Figure 8 we show the simple subtraction of the spectrum of sea water from that of pure water. The effect of salts is to introduce a third water structure that is contained in the solvation shell around an ion, the quantity of which is independent of temperature and pressure. This is well known as the haline contraction effect in describing the physical properties of sea water.

For a typical cation six water molecules are arranged as a regular octahedron as in $[Na(H_2O)_6]^+$ with the water oxygen atom oriented to be adjacent to the metal ion. The effects for anions are far less well known and with the water molecule orientation reversed. The cationic water molecules are bound, but not hydrogen bonded; technically they form a dative covalent bond between the oxygen atom and the metal ion similar to a metal-ligand complex. The water molecules are singular, but not free, their vibrational modes are restricted, and their polarity is likely reduced by proximity to the ion, thus their Raman cross section is likely less than that of the free nHB form. In addition, because their vibrational modes are restricted as compared to the free singlet water molecules, their Raman shift is likely different as well. Unfortunately, due to their low concentration and reduced Raman cross section, we have yet to deconvolve these bands as separate Gaussian peaks. Their effect, however, can be seen in the slight differences in the Raman shift of peaks 3 and 4 versus the Raman shift of those peaks in pure water (see Table 1).

The concentration of water in water is ~55.5 M; the total quantity of ions in sea water (S_p = 34.348 as used here) is 1.125 M (Millero, 1974). If we take a

Table 3
Composition of 1 Kg of Sea Water as a Function of Chlorinity[a,b]

Ion	g_i/Cl(‰) (g)	n_i/Cl(‰) (moles)	e_i/Cl(‰) (eq)	Mass[c] (g)	Concentration (moles/kg)	Concentration (moles/L)[d]
Na^+	0.55556	0.0241655	0.0241655	10.5629	0.459459	0.470608
Mg^{2+}	0.06680	0.0027484	0.0054968	1.2701	0.052255	0.053523
Ca^{2+}	0.02125	0.0005302	0.0010604	0.4040	0.010081	0.010325
K^+	0.02060	0.0005268	0.0005268	0.3917	0.010016	0.010259
Sr^{2+}	0.00041	0.0000047	0.0000094	0.0078	0.000089	0.000092
Cl^-	0.99894	0.0281765	0.0281765	18.9928	0.535720	0.548719
$SO_4^=$	0.14000	0.0014575	0.0029149	2.6618	0.027710	0.028383
HCO_3^-	0.00735	0.0001205	0.0001205	0.1397	0.002291	0.002347
Br^-	0.00348	0.0000436	0.0000436	0.0662	0.000829	0.000849
F^-	0.00006	0.0000035	0.0000035	0.0011	0.000067	0.000068
Sum Cations	0.66462	0.0279756	0.0312589	12.6364	0.531900	0.544807
Sum Anions	1.14983	0.0298016	0.0312590	21.8617	0.566617	0.580366
Sum Ions	1.81445	0.0577772	0.0625179	34.4981	1.098517	1.125173
$B(OH)_3$	0.00132	0.0000213	0.0000213	0.0251	0.000405	0.000415
Totals	1.81577	0.0577985	0.0625392	34.5232	1.098922	1.125588

[a]Ion-chlorinity ratios are from Table 1 in Millero (1974). [b]UNESCO definition of salinity = 1.80655 * Cl (‰); so, Cl (‰) = S_P/1.80655. [c]For a seawater sample with S_P = 34.348, Cl (‰) = 19.013. [d]Based upon a density of 1.0243 g/mL at 20 °C.

canonical value of 6 water molecules around each cation ion, then some 6% of water in sea water is bound in this form. For anions the situation is far less clear. Walrafen (1964) carried out early studies on the effect of added salts on water structure finding that "O-H···O units were broken (in varying degrees) in all cases." He noted that "certain anions are particularly effective …". He concluded that "the Raman spectrum is insensitive to effects produced by hydration of (some) cations, but it is very sensitive to the effects resulting from the hydration of certain anions, e.g., Br^-." Yet modern studies reverse this finding and attribute the dominant changes to cation solvation and find only minimal or no changes in water structure from the presence of anions. We provide this historical note here only to illustrate the difficulty in accurately addressing this problem, and to show how thinking has evolved over time.

There is today a huge literature on the solvation shells around ions in aqueous solution, but very little of this is usefully applicable to the ocean sciences; almost all studies are on the effects of individual salts, and the effects of ion pairing, prominent in sea water, are not well known. Discussions of inner- and outer-shell solvation, and water structure makers and structure breakers abound, but we have not found these to be helpful here (Horne, 1969). Possibly the most helpful descriptions are contained in the X-ray Raman papers by Waluyo et al. (2011, 2014). Here it is reported that "Cl^- and Br^- are shown to have insignificant effect on the structure of water" whereas the measurements "confirm the H-bond breaking effect of Na^+ and the effect on the liquid as similar to an increase in temperature." This description should not be taken to mean that the ions draw molecules exclusively from the HB pool, as does a rise in temperature; it is simply that the HB pool is far greater and so this is the dominant source drawn upon.

The practical result is that it is helpful to consider the molecules in the solvation shell as simply sequestered from the bulk fluid in a quantity linearly related to salinity. There is clear evidence for the role of cations and much uncertainty over the role of anions. The remaining molecules in the bulk fluid then are partitioned solely as a function of *T* in ratios identical to that in pure water. This provides a simple explanation of the exactly parallel lines of the effects of temperature and salinity found in the simple two-component model of Becucci et al. (1999).

The need here is to provide a more quantitative estimate of the molecular population in sea water as a function of salinity. The maximum quantity would be to have six water molecules in the first solvation shell around each cation and anion. The best estimates from recent work (Waluyo et al., 2014) suggest that the H bonds are broken only by cations, reducing the bound water estimate by 50%. An average of the two would suggest 4.5 ± 1.5 molecules per ion. Yet the effects of ion pairing are not included here, and this is common in the major ions of sea water with species such as Mg-SO_4 and Mg-CO_3 being prominent.

Table 4
The Quantities of Hydrogen Bonded (HB) and nHB Forms in Sea Water of 34.348 Salinity Based Upon the van 't Hoff Relationship for Pure Water (Table 2) and Corrected for the Quantity of Water Estimated as Bound in the Solvation Shell Around Cations

S pss-78	*T* °C	Density g/cm^3	PW % HB[a]	Conc (moles/L)			Mole-%		
				[HB][b]	[nHB][c]	[Solv][d]	[HB]	[nHB]	[Solv]
34.348	0.00	1.0276	90.00	46.61	5.18	3.28	84.64	9.40	5.95
34.348	10.00	1.0264	88.36	45.71	6.02	3.28	83.09	10.95	5.95
34.348	20.00	1.0243	86.62	44.71	6.91	3.27	81.46	12.59	5.95
34.348	30.00	1.0212	84.80	43.65	7.82	3.26	79.75	14.30	5.95
34.348	40.00	1.0175	82.92	42.52	8.76	3.25	77.98	16.07	5.95

Note. For sea water of S_P = 34.348, S_A = 34.524 g/kg, ∑cations = 0.5319 moles/kg.
[a]Percent nHB was calculated from the regression in Figure S1.2; percent HB = 100 - nHB. [b]HB (moles/L) = (1,000 g − mass of salt)/mw of H_2O − moles of solvation H_2O) × density(S,T) × % HB. [c]nHB (moles/L) = (1000 g − mass of salt)/mw of H_2O − moles of solvation H_2O) × density(S,T) × (100 − % HB). [d]moles of solvation H_2O = 6 × moles of cations/kg.

For the purposes of this paper we will (with caution) adopt the Waluyo et al. (2014) "cations only" estimate and take a value of 6 moles of water sequestered in the solvation shells per mole of cations in sea salt. It is likely that this estimate can be improved with further work on the Raman cross sections. If this estimate is correct then the molar quantities of the HB and nHB forms reported in Table 2 for pure water can simply be adjusted for the sea water of practical salinity 34.348 via the information in Table 3. That is, since the sum of cations is 0.545 M, then some 3.27 M of water out of a total of 55.5 M (5.89%) are sequestered into the solvation shell. We do not know this number precisely, but an adjustment of 6% for the sequestering of water by solvation seems practical at this time.

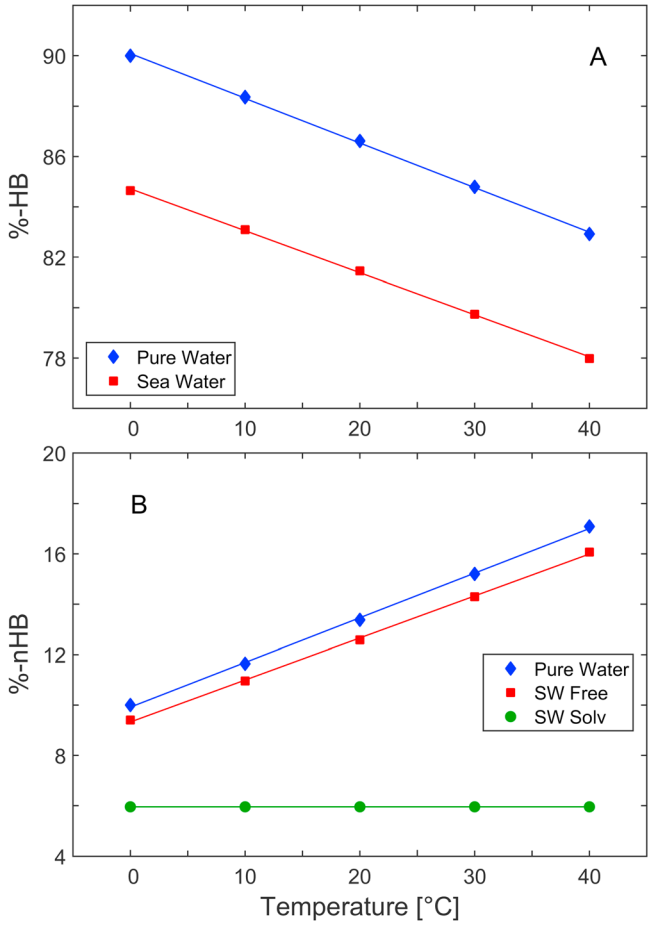

Figure 9. Plots of the calculated percent abundance of both the hydrogen bonded form (a) and the nHB forms (b) for pure water (blue line) and for sea water (red line) at 1 atm as a function of temperature. The green line in (b) shows the concentration of water sequestered within the solvation shells of the cations in sea salt. HB = hydrogen bonded; nHB – nonhydrogen bonded.

In Table 4 we present the approximate molar concentrations and percent of the HB, nHB, and solvation water forms in sea water (S_P = 34.348). In Figure 9 we show the estimated percent abundances of the HB and nHB forms in pure water and sea water of the same salinity.

From observation of the effect of salinity in reducing the overall abundance of pentamer forms as water molecules are sequestered within the solvation shells of cations, we would expect that sea water would be less compressible than pure water due to the loss of the pentamers that are subject to the nesting process (Canpolat et al., 1998), and this is the case (Bradshaw & Schleicher, 1976; Millero & Huang, 2011). As noted earlier this effect is also manifest in the fact that warm water, with a greater abundance of single water molecules, is less compressible than is cold water.

We do not have direct spectroscopic evidence of the effects of pressure, since this has only a small effect on hydrogen bonding. But pressure effects are important in the ocean sciences and so we should seek some way to quantify the pentamer nesting model of Canpolat et al. (1998) shown in Figure 10 and examine how large the effect on the population might be. One simple way is to examine the correlation with the effects of pressure on the speed of sound. The compressional wave of a sound pulse forces water molecules into closer proximity, just as does hydrostatic pressure. Sound speed and sound absorption are correlated (Stokes, 1845) and we have recently shown (Brewer et al., 2015) that the speed of sound in sea water can be simple and well represented as a van 't Hoff function, implying control by chemical equilibria within the water molecular system.

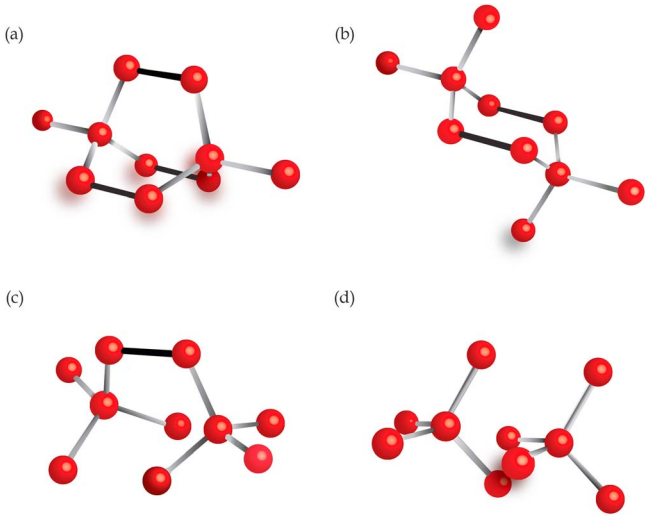

Figure 10. Examples of four possible local energy minima of two adjacent pentamers under pressure (redrawn from Canpolat et al., 1998). The darker lines indicate interpentamer hydrogen bonds, the lighter lines the normal intrapentamer hydrogen bonds. Only configuration (d)—the nesting of pentamers—yields a reduction in volume and is achieved with no additional hydrogen bonding. This form is fully consistent with both our field and laboratory experiments on the structure of water in sea water under pressure. This depicts a simple nearest neighbor model.

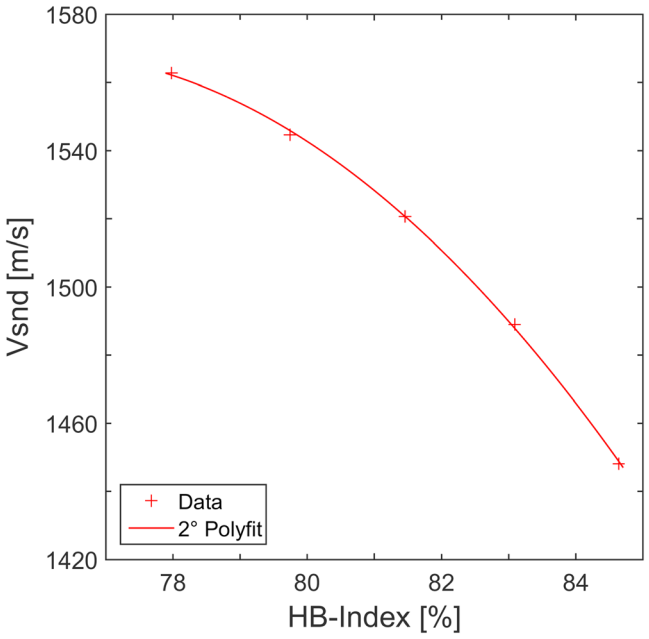

Figure 11. Plot of the speed of sound in sea water at 1 atm total pressure and constant salinity (S_A = 34.524) versus the percentage of HB forms present as calculated in Table 4 over a range of temperatures. A simple quadratic equation provides an excellent fit (see supporting information for coefficients).

The simplest physical explanation of this is to consider that sound speed is slowed in colder water by the force required to nest pentamers; this takes both work and time. In warm water, with the presence of fewer pentamers, there is less to impede the sound wave; and under higher hydrostatic pressure the population of individual pentamers is reduced since many are already forced into proximity, and again, there is less to impede the sound wave. Thus, both warmer water and increased pressure act to increase sound speed and decrease sound absorption. The sequestration of some water molecules into the solvation shell is also the reason why sound speed in sea water is faster than that in pure water.

One manifestation of this is that the typical ocean water column sound speed minimum depth should be closely correlated with the water column $(H_2O)_5$ maximum, and this should be a testable hypothesis. For a specific example, we examine the water column at station 10 of the hydrographic line WOCE P17N, with acoustic characteristics earlier described by us (Brewer et al., 2015). Here the sound speed at 4,000-m depth slightly exceeds that at the surface. In surface ocean waters sound speed and the estimated molar concentration of water pentamers are well correlated (Figure 11). Simply extrapolating this function to depth results in a large underestimation of sound speed; but if only ~2% of the water pentamers are removed at 4,000 m by the pressure-induced nesting process, then a very reasonable fit can be obtained.

One further example where knowledge of water molecular structure may have useful application in ocean science is in the understanding of thermobaricity and cabbeling (McDougall, 1987). These processes can result in advection of tracer properties across neutral density surfaces when some water masses mix due to nonlinearities in the equation of state of sea water. Today these are known only as derivations from bulk fluid coefficients as in $\delta^2\rho/\delta\theta\delta\rho$ (thermobaricity) or $\delta^2\rho/\delta\theta^2$ (cabelling). Changes in *T* and *P* both have the capacity to change the volume of the fluid; yet the molecular processes that drive changes in density from temperature and pressure perturbations are profoundly different. While a detailed description of these properties is beyond the scope of this paper, the basic rules of change in compressibility with temperature and the saline contraction coefficient, have their origins in the changing molecular properties, and in particular in the abundance of the $(H_2O)_5$ species as a function of *S*, *T*, and *P*. The information presented here is a first attempt to address this.

6. Conclusions

We hope that the introduction to the chemical physics of water in sea water presented here is useful in opening the door to a representation of the physical properties of sea water in terms of the molecular properties of water itself. It would, for example, be difficult to comprehend ocean CO_2 chemistry if one was not aware that it was driven by the pH dependence of the HCO_3, CO_3, and CO_2 species. Yet most ocean scientists are unaware of the temperature-dependent equilibrium of the principal water species as primary controls on the physical properties of sea water.

In making the translation from Raman spectroscopy of pure water to sea water, it is the formation of the third form of water in the solvation shell around an ion that introduces the largest uncertainty. We have been able to estimate the abundance of the HB and nHB forms in the bulk fluid, but the Raman cross section of water in the solvation shell and the Raman shift

of the two stretching modes of these water molecules are not known. Since the molecules here are likely less polarized it seems possible that the Raman cross section is reduced compared to the nHB single molecules in the bulk fluid.

Nowhere in the ocean, apart from the extreme conditions in hydrothermal vents (Li et al., 2018), do we find that the concentration of the simple nHB H_2O molecule exceeds 20% of the total water forms. Over 80% exists as versions of the HB forms, dominantly as the $(H_2O)_5$ pentamer.

Much remains to be tested, but it seems likely that it is the quantity of the pentamer form that controls many of the physical properties of sea water such as sound speed and sound absorption, compressibility, etc. (IOC et al. 2010). And it is likely that it is the abundance of the single H_2O molecule that controls mineral dissolution, water transfer across cell walls, and across the air-sea interface. The transport of ionic species across cell membranes is accompanied by associated water molecules in a modified solvation shell with remarkable increases in efficiency (Peng et al., 2018). Some of this is implicit in the way that temperature and pressure-dependent formulae are written today, but the direct representation of the equilibrium state of water in natural waters appears to be a more natural and teachable approach.

The fidelity of the simple van 't Hoff equation in representing the proportions of the major water species present is remarkable, and this relationship seems to provide a master control. The end result is that by far the dominant molecule in the oceans is the $(H_2O)_5$ pentamer representing some 78–85% of water in sea water depending on temperature. Some 6%—possibly more—is present in the solvation shell surrounding an ion, and this quantity does not depend upon temperature but only on salinity. The abundance of the free H_2O molecule is quite small, perhaps 9–16%, again dependent on temperature and salinity. The effect of pressure is most simply expressed as a nesting of the pentamer forms, but no hydrogen bonds are broken in this process and we cannot observe this spectroscopically—it is a result from molecular dynamics modeling reported by others for pure water, and this formulation appears to apply to sea water.

Acknowledgments
This work was supported by a grant to the Monterey Bay Aquarium Research Institute by the David and Lucile Packard Foundation. We thank J. W. Murray and J. G. Shepherd for helpful and informed comments on the manuscript. We thank David Jumes for his help with laboratory Raman measurements. We thank the crew of the RVs *Western Flyer* and *Rachel Carson*, and the pilots of the ROVs *Doc Ricketts* and *Ventana*, for their skilled assistance at sea.

References

Becucci, M., Cavalieri, S., Eramo, R., Fini, L., & Materazzi, M. (1999). Accuracy of remote sensing of water temperature by Raman spectroscopy. *Applied Optics*, *38*(6), 928–931. https://doi.org/10.1364/AO.38.000928

Bradshaw, A., & Schleicher, K. (1976). Compressibility of distilled water and seawater. *Deep Sea Research, Part I*, *23*, 583–593.

Brewer, P. G., Malby, G., Pasteris, J. D., White, S. N., Peltzer, E. T., Wopenka, B., et al. (2004). Development of a laser Raman spectrometer for deep-ocean science. *Deep-Sea Research Part I*, *51*(5), 739–753. https://doi.org/10.1016/j.dsr.2003.11.005

Brewer, P. G., Peltzer, E. T., Ryan, J., Kirkwood, W. J., & Hofmann, A. F. (2015). Ocean chemistry and the speed of sound in sea water. *Marine Chemistry*, *177*, 591–606. https://doi.org/10.1016/j.marchem.2015.09.009

Brewer, P. G., Peltzer, E. T., Walz, P. M., & Wojciechowicz, M. (2017). The speciation of water in sea water and in gelatinous marine animals. *Marine Chemistry*, *195*, 94–104. https://doi.org/10.1016/j.marchem.2017.05.002

Canpolat, M., Starr, F. W., Scala, A., Reza Sadr-Lahijany, M., Mishima, O., Havlin, S., & Stanley, H. E. (1998). Local structural heterogeneities in liquid water under pressure. *Chemical Physics Letters*, *294*(1-3), 9–12. https://doi.org/10.1016/S0009-2614(98)00828-8

Carey, D. M., & Korenowski, G. M. (1998). Measurement of the Raman spectrum of liquid water. *The Journal of Chemical Physics*, *108*(7), 2669–2675. https://doi.org/10.1063/1.475659

Furić, K., Ciglenec˘ki, I., & C´osovic´, B. (2000). Raman spectroscopic study of sodium chloride water solutions. *Journal of Molecular Structure, 550–551*, 225–234.

Horne, R. A. (1969). *Marine chemistry* (p. 568). New York: Wiley.

IOC, SCOR, IAPSO (2010). The international thermodynamic equation of seawater—2010: Calculation and use of thermodynamic properties. *Intergovernmental Oceanographic Commission Manuals and Guides 56*. UNESCO (English) (182 pp.). Retrieved from http:// www.TEOS-10.org

Keutsch, F. N., & Saykally, R. J. (2001). Water clusters: Untangling the mysteries of the liquid, one molecule at a time. *Proceedings of the National Academy of Sciences of the United States of America*, *98*(19), 10,533–10,540. https://doi.org/10.1073/pnas.191266498

Khoshtariya, D. E., Zahl, A., Dolidze, T. D., Neubrand, A., & van Eldik, R. (2004). Local dense structural heterogeneities in liquid water from ambient to 300 MPa pressure: Evidence for multiple liquid-liquid transitions. *Chemphyschem*, *5*(9), 1398–1404. https://doi.org/10.1002/cphc.200400219

Kumar, R., Schmidt, J. R., & Skinner, J. L. (2007). Hydrogen bonding definitions and dynamics in liquid water. *The Journal of Chemical Physics*, *126*(20), 204107. https://doi.org/10.1063/1.2742385

Leonard, D. A., Caputo, B., & Hoge, F. E. (1979). Remote sensing of subsurface water temperature by Raman scattering. *Applied Optics*, *18*(11), 1732–1745. https://doi.org/10.1364/AO.18.001732

Leonard, D. A., Caputo, B., Johnson, R. L., & Hoge, F. E. (1977). Experimental remote sensing of subsurface temperature in natural ocean water. *Geophysical Research Letters*, *4*, 279–281. https://doi.org/10.1029/GL004i007p00279

Li, L., Zhang, X., Luan, Z., Du, Z., Xi, S., Wang, B., et al. (2018). In situ quantitative Raman detection of dissolved carbon dioxide and sulfate in deep-sea high-temperature hydrothermal vent fluids. *Geochemistry, Geophysics, Geosystems*, *19*, 1809–1823. https://doi.org/10.1029/2018GC007445

McDougall, T. J. (1987). Thermobaricity, cabbeling, and water-mass conversion. *Journal of Geophysical Research*, *92*, 5448–5464. https://doi.org/10.1029/JC092iC05p05448

Millero, F. J. (1974). Seawater as a multicomponent electrolyte solution. In E. D. Goldberg (Ed.), *The Sea*, *Marine Chemistry* (Vol. 5, pp. 3–80). New York: Wiley.

Millero, F. J., & Huang, F. (2011). The compressibility of sea water from 0 to 95°C at 1 atm. *Marine Chemistry*, *126*(1-4), 149–154. https://doi.org/10.1016/j.marchem.2011.05.003

Mishima, O., & Stanley, E. H. (1998). The relationship between liquid, supercooled and glassy water. *Nature*, *396*(6709), 329–335. https://doi.org/10.1038/24540

Pauling, L. (1960). *The nature of the chemical bond*. Ithaca, New York: Cornell University Press.

Peltzer, E. T., Zhang, X., Walz, P. M., Luna, M., & Brewer, P. G. (2016). In situ Raman measurement of HS^- and H_2S in sediment pore waters and use of the HS^-:H_2S ratio as an indicator of pore water pH. *Marine Chemistry*, *184*, 32–42. https://doi.org/10.1016/j.machem.2016.05.006

Peng, J., Cao, D., He, Z., Guo, J., Hapala, P., Ma, R., et al. (2018). The effect of hydration number on the interfacial transport of sodium ions. *Nature*, *557*(7707), 701–705. https://doi.org/10.1038/s41586-018-0122-2

Purcell, E. M. (1976). Life at low Reynolds number. *American Journal of Physics*, *45*, 3–11.

Robinson, G. W., Cho, C. H., & Urquidi, J. (1999). Isobestic points in liquid water: Further strong evidence for the two-state mixture model. *The Journal of Chemical Physics*, *111*(2), 698–702. https://doi.org/10.1063/1.479349

Silverstein, K. A., Haymet, A. D. J., & Dill, K. A. (2000). The strength of hydrogen bonds in liquid water and around nonpolar solutes. *Journal of the American Chemical Society*, *122*(33), 8037–8041. https://doi.org/10.1021/ja000459t

Smith, J. D., Cappa, C. D., Wilson, K. R., Cohen, R. C., Geissler, P. L., & Saykally, R. J. (2005). Unified description of temperature-dependent hydrogen-bond rearrangements in liquid water. *Proceedings of the National Academy of Sciences of the United States of America*, *40*, 14,171–14,174.

Stanley, E. M., & Batten, R. C. (1969). Viscosity of sea water at moderate temperatures and pressures. *Journal of Geophysical Research*, *74*, 3415–3420. https://doi.org/10.1029/JC074i013p03415

Stokes, G. G. (1845). On the theories of the internal friction of fluids in motion and of the equilibrium and motion of elastic solids. *Transactions of the Cambridge Philosophical Society*, *8*, 287–319.

Walrafen, G. E. (1964). Raman spectral studies of water structure. *The Journal of Chemical Physics*, *40*(11), 3249–3256. https://doi.org/10.1063/1.1724992

Walrafen, G. E. (1967). Raman spectral studies of the effects of temperature on water structure. *The Journal of Chemical Physics*, *47*(1), 114–126. https://doi.org/10.1063/1.1711834

Walrafen, G. E., Hokmadabi, M. S., & Yang, W.-H. (1986). Raman isosbestic points from liquid water. *The Journal of Chemical Physics*, *85*(12), 6964–6969. https://doi.org/10.1063/1.451383

Waluyo, I., Huang, C., Nordlund, D., Bergmann, U., Weiss, T. M., Pettersson, L. G. M., & Nilsson, A. (2011). The structure of water in the hydration shell of cations from X-ray Raman and small angle scattering measurements. *The Journal of Chemical Physics*, *134*(6), 064513. https://doi.org/10.1063/1.3533958.

Waluyo, I., Nordlund, D., Bergmann, U., Schlesinger, D., Pettersson, L. G. M., & Nilsson, A. (2014). A different view of structure-making and structure-breaking in alkali halide aqueous solutions through X-ray absorption spectroscopy. *The Journal of Chemical Physics*, *140*(24), 244506. https://doi.org/10.1063/1.4881600

Zhang, X., Hester, K. C., Ussler, W., Walz, P. M., Peltzer, E. T., & Brewer, P. G. (2011). In situ Raman-based measurements of high dissolved methane concentrations in hydrate-rich ocean sediments. *Geophysical Research Letters*, *38*, L08605. https://doi.org/10.1029/2011GL047141

Zhang, X., Kirkwood, W. J., Walz, P. M., Peltzer, E. T., & Brewer, P. G. (2012). A review of advances in deep-ocean Raman spectroscopy. *Applied Spectroscopy*, *66*(3), 237–249. https://doi.org/10.1366/11-06539